Sensor and Simulation Notes

Note 434

**Recent Enhancements to the
Multifunction IRA and TEM Sensors**

Leland H. Bowen
Everett G. Farr
Farr Research, Inc.

February 1999

Abstract

In Sensor and Simulation Note 413 we described two new antennas, a Multifunction Impulse Radiating Antenna (MIRA), and a TEM sensor. Since then, several improvements have been made to both the MIRA and TEM sensor. These improvements have greatly enhanced the measurement accuracy of the sensor and the response of the MIRA. These improvements also enhanced the structural stability and durability of both antennas. In this note we describe the improvements that were implemented, and we provide new data demonstrating the enhanced performance.

I. Introduction

A reflector Impulse Radiating Antenna (IRA) consists of a paraboloidal reflector with a TEM feed. This antenna has a beamwidth which is too narrow for some applications, so to broaden the beam, the Multifunction IRA or MIRA was introduced in [1]. In that paper a MIRA was built and tested using TEM sensors. These TEM sensors, which replicate the incoming field, were developed to enhance the signal-to-noise ratio with very fast, low voltage pulsers.

The first versions of both the TEM sensors and the MIRA left some room for improvement. In particular, the TDRs of both of these antennas were not as flat as they could have been, due to an imperfect impedance match, especially near the feed points. In the improved versions, the TDR has been significantly improved. In addition, structural modifications have been implemented that make the antennas considerably more sturdy and suitable for field use.

The modifications to the two antennas are described in the following sections. New experimental data are provided to show the effects of the modifications. The experimental setup for the measurements in this paper is the same as that used in [1(Fig. 4.4)]. The source was a PSPL 4015C step generator with a risetime of 20 ps. The received signal was sampled by an SD24 sampling head and a Tektronix 11801B Digital Sampling Oscilloscope.

II. TEM Sensor Enhancements

We begin with the TEM sensor enhancements. The original TEM sensor was essentially a half TEM horn mounted against a truncated ground plane [1(Fig. 4.3)]. The ground plane was a 10 x 24 inch aluminum plate. The conical plate was tin-plated copper supported by a block of styrofoam. The modifications to the sensor included replacing the foam support with solid teflon posts, and improvements to the feed point. The TDR of the improved 50 Ω sensor is shown in Figure 2.1. Note that the TDR is very flat near the feed point, almost to the point where the feed point is not detectable. This results in much improved measurement accuracy.

We also built a 100 Ω version of the TEM sensor, in order to improve its sensitivity. The new 100 Ω sensor is shown in Figure 2.2. The calibration of the sensor is carried out in accordance with [2], and the results are shown in Figures 2.3 – 2.6. The TDR is shown in Figure 2.7. Figures 2.3 – 2.7 correspond to Figures 4.6 – 4.10 of [1].. Changing the impedance of the TEM sensor from 50 to 100 Ω increases the sensitivity, due to the increased effective height. While the 100 Ω sensor has a an impedance mismatch to the 50 Ω cables, the improvement in sensitivity more than offsets the effect of the mismatch. The aperture height of the original antenna was 31 mm, and the effective height was 17 mm [1]. The modified sensor has an aperture height of 63.5 mm, and an effective height of 23 mm as calculated from Figure 2.6 [2, Eqn. 3.3].

The height of the feed element above the ground plane must be carefully controlled, in order to maintain a constant impedance. During construction of the original sensor, it was found that cutting the foam supports with high accuracy was not practical. Also, the foam supports did not keep the top plate firmly in place if the sensor was bumped, a common occurrence in the field. In the redesigned sensors the foam was replaced with teflon support posts held in place with nylon screws. The post locations can be seen in the TDRs of Figures 2.1 and 2.7, but their effect is extremely small, due to the low relative dielectric constant of teflon (e_r = 2.2) and the small amount of material used. It was found that accurate adherence to the theoretical width-to-height ratio is necessary, except near the feed point, where the plate thickness becomes a greater consideration. Near the feed point the height of the plate above the ground point must be increased, to maintain the desired impedance and a flat TDR.

At the feed point, it was found that connecting the center pin of the feed-through connector as close as possible to the apex of the triangle improved the TDR of the antenna substantially. Also, it was determined that keeping excess metal around the connector/feed element interface to a minimum improved the TDR at the feed point. Some extra metal is required, however, for mechanical strength and soldering. The aluminum ground plane was finished with clear alodine and the copper feed element was gold plated to prevent corrosion and maintain high conductivity.

The 50 and 100 Ω sensors described here have been very useful in characterizing several antennas in addition to the MIRA. These sensors have a measurement clear time of 2 ns. For some antennas, it is necessary to measure the response at later times, so larger TEM sensors were developed that have a measurement clear time of 4 ns. Table 2.1 lists the characteristics of the TEM sensors, which are now all commercially available. The ground planes are 10 x 24 inches

for the small sensors and 20 x 48 inches for the large sensors. These sensors were characterized using the method of two identical antennas.

Table 2.1. TEM Sensors Developed by Farr Research

Model Number	Size	Impedance (Ω)	FWHM ps	h_{eff}* mm	3 dB freq. GHz	Clear Time ns
FRI-TEM-01-50	Small	50	31	17	12	2
FRI-TEM-01-100	Small	100	36	23	10	2
FRI-TEM-02-50	Large	50	40**	30	7**	4
FRI-TEM-02-100	Large	100	47	42	6	4

* $V_{out}(t) \approx h_{eff}\ E_{inc}(t)$.
**   Estimated.
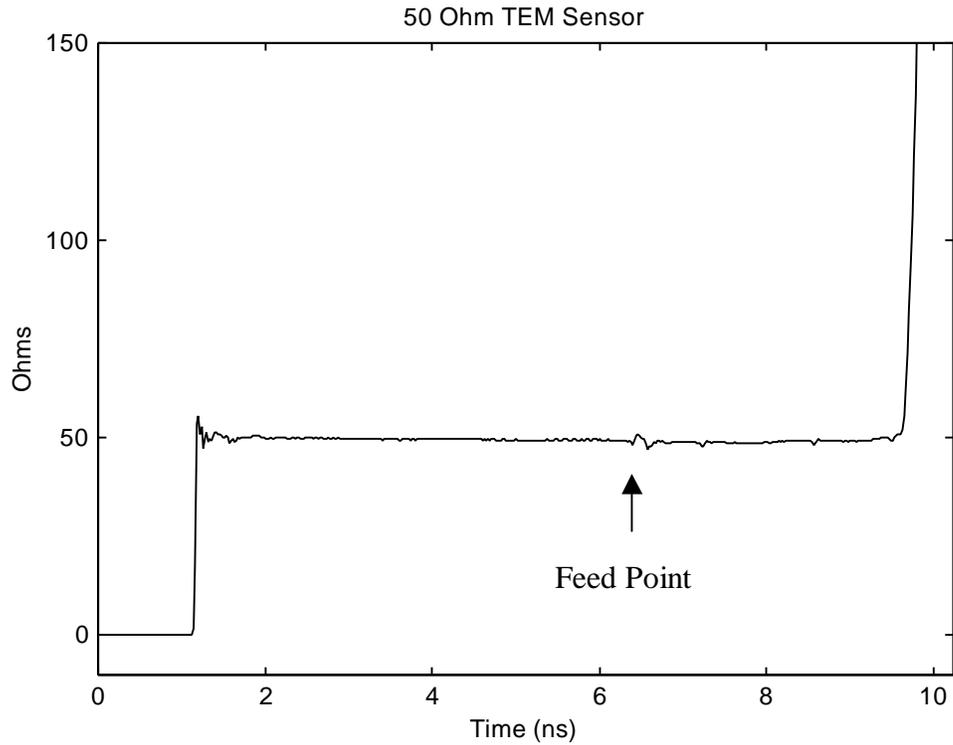
Figure 2.1. TDR of the 50 Ω TEM Sensor.

Figure 2.2. 100 Ω TEM Horn Sensor
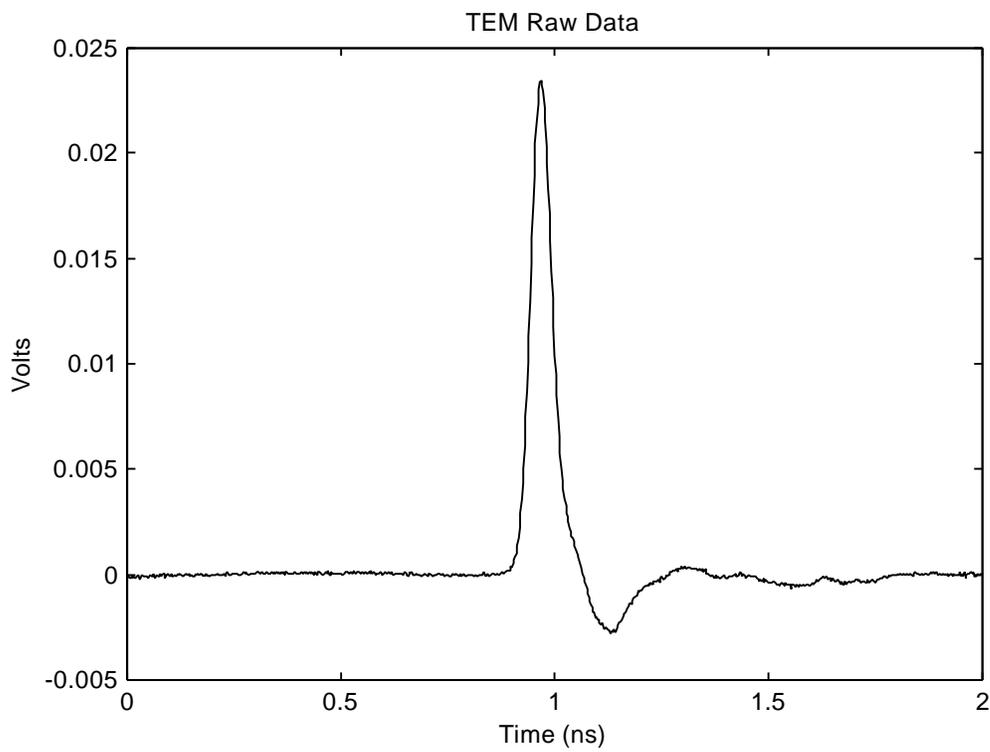
Figure 2.3. Raw Received Waveform for TEM Sensor Calibration, using two identical sensors (FWHM = 57ps).

TEM Sensor, Impulse Response
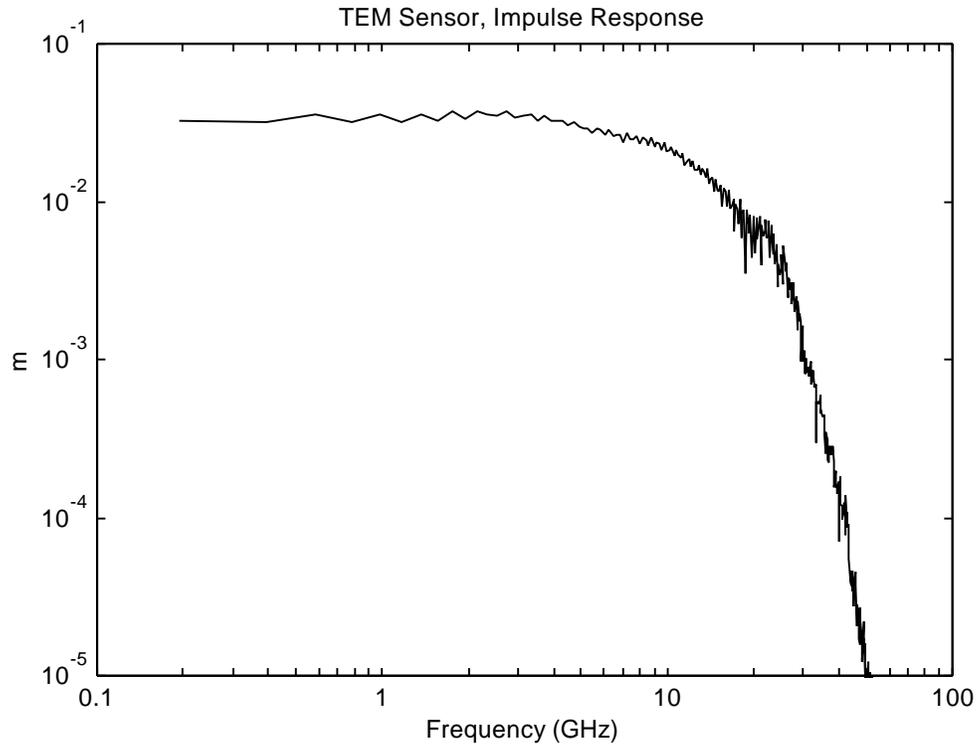
Figure 2.4. TEM sensor impulse response, $h_{tem}(w)$, in the frequency domain.

TEM Sensor, Impulse Response, (htem)
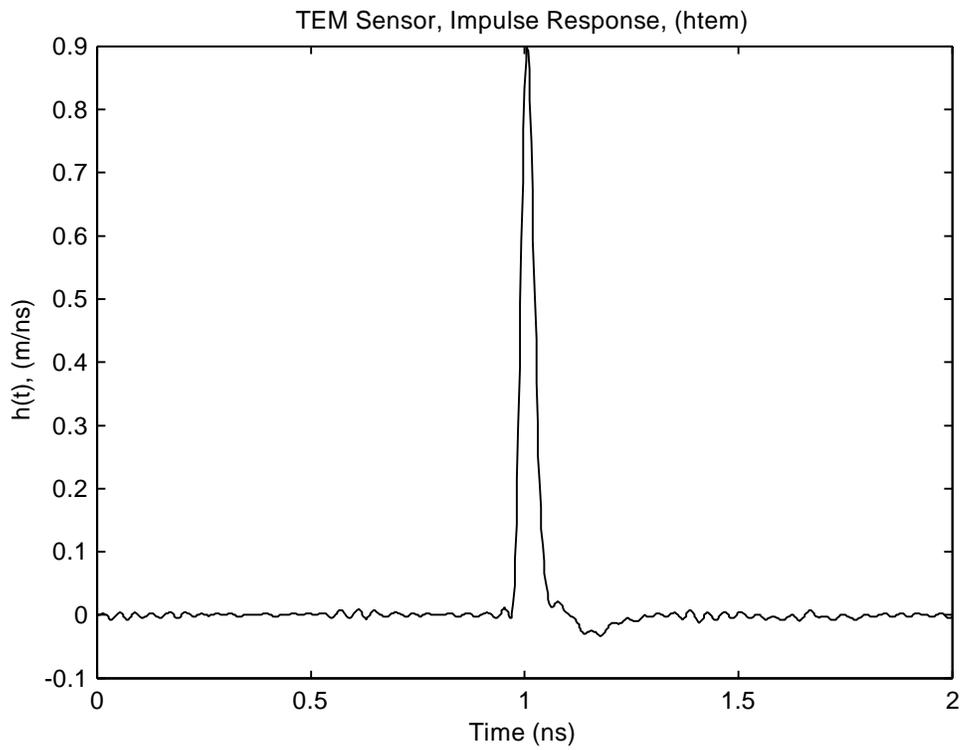
Figure 2.5. TEM sensor impulse response, $h_{tem}(t)$, in the time domain (FWHM = 35ps).

TEM Sensor, Integrated Impulse Response
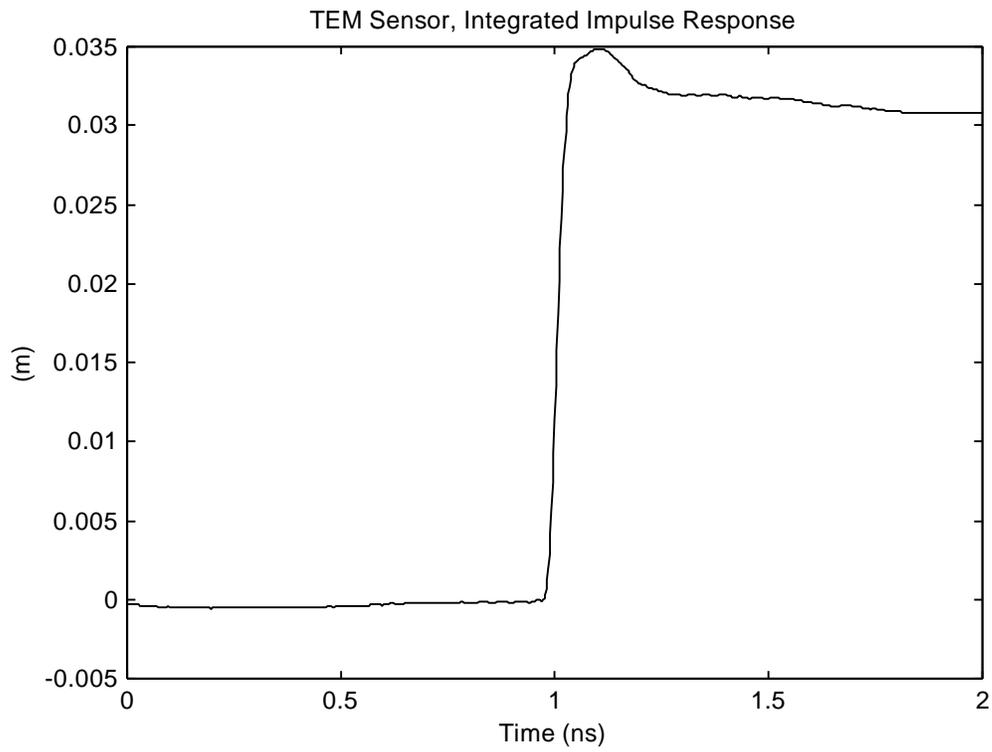
Figure 2.6. Integral of the TEM sensor impulse response.
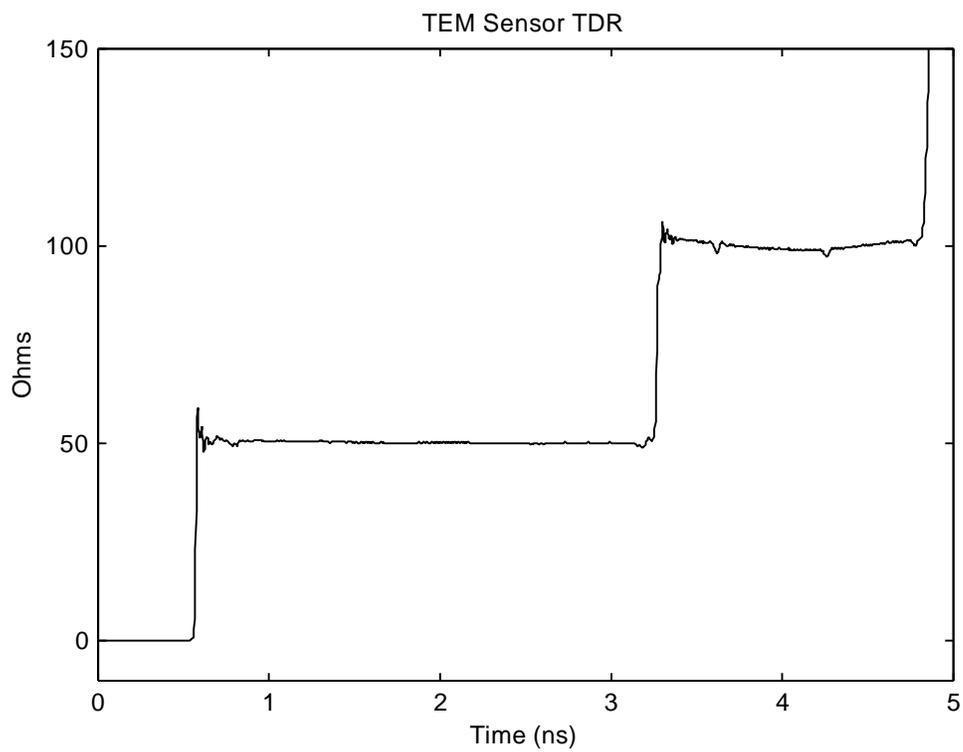
TEM Sensor TDR

Figure 2.7. TDR of the 100 Ω TEM Sensor.

III. MIRA Enhancements

Let us now consider enhancements to the MIRA. Modifications to the MIRA included refinement of the feed point and replacement of the feed arms and support structure. The original MIRA design [1(Figs. 4.1–4.2)] had feed elements that were 1/8 in. thick and had two large bumps near the feed point. One bump provided space for a screw hole for attaching the feed element to a plastic support at the apex. The other bump provided space for a soldering hole for attaching the coax feed cable. By reducing the thickness of the feed arms to 1/16 in. and by eliminating the bumps in the feed arms, the TDR at the feed point was greatly improved. Also, the plastic support structure at the apex was replaced with UHMW polyethylene supports, located about one-third of the distance from the apex to the load resistors. While the new supports increased the amount of plastic present, they made it possible to build the feed point much smaller. The thinner feed arms reduced aperture blockage, and they also helped to maintain a flat TDR near the feed point. Considerable care was used when rebuilding the MIRA, to keep the two feed cables exactly the same length, and to keep the exposed center conductors at the apex as short as possible.

The modified MIRA is shown in Figure 3.1. The data taken on this improved MIRA is shown in Figures 3.2 – 3.9, and these figures correspond to Figures 4.11–4.13 in [1]. The raw voltage for the receive signal is shown in Figure 3.2, which corresponds to [1(Fig. 4.11)]. The double spike that appeared in the original data was eliminated by our modifications. The FWHM of the raw voltage response is 80 ps.

We next processed the data to find the MIRA's impulse response, $h(t)$, by deconvolving the sensor and system response [2(Eqn. 8.1)]. The resulting impulse response, shown in Figures 3.3 and 3.4, has a FWHM of 51.3 ps. This impulse response was then integrated, as shown in Figure 3.5. The jump in the integral corresponds to the aperture height, h_a, which in this case is 100 mm. The theoretical value for an 18-inch diameter IRA ($r = 228.6$mm) is 149 mm, using the formula $h_a = 0.92\, a/\sqrt{2}$, where a is the reflector radius [3]. So the experimental h_a is 67% of the theoretical value.

Next, we measured the MIRA's antenna pattern in the H-plane. The raw voltage response of the MIRA is shown Figures 3.6 – 3.8 for $f_f = F_2/F$ set to 1.0, 0.85, and 0.70. Measurements were taken at 0°, 7.5°, and 15° off boresight in the H-plane. Table 4.1 shows the Half Field Beam Widths (HFBW) for the modified MIRA.

Table 4.1. MIRA Half Field Beam Widths

$f_f = F_2/F$	H-Plane Half Field Beam Widths (HFBW)	
	Theory [1]	Measurement
1.00	8°	15°
0.85	15°	26°
0.70	36°	42°

In Section III of [1] the normalized field on boresight is calculated to be $rE/V_0 = 6.2$ for the focused ($f_f = 1.0$) case. To compare the new data with this theoretical value we must

normalize the peak voltage value from Figure 3.2. The normalization factor is $(V_0 \times h_{eff}/r)$, where $V_0 = 4$ V, $r = 3.2$ m, and $h_{eff} = 0.023$ m. This gives a value of 28.7 mV. The normalized peak voltage from Figure 3.2 is then 74 mV / 28.7 mV = 2.58, which is 41% of the predicted value. This is an improvement of almost 10% from the previous data. However, it is still low, due in part to the possibility that the measurements were taken at the edge of the near field, and due in part to pulse spreading. Note that the measured h_a, which is the integral of the impulse response, is a better fit to the theory (67%).

Figure 3.9 shows the TDR for the modified MIRA. The improvement over the TDR in Figure 4.13 of [1] may not be readily apparent, due to the change in the vertical axis from volts to ohms. However, the sharp jump in impedance at the feed point has been reduced from almost 90 Ω to below 70 Ω.
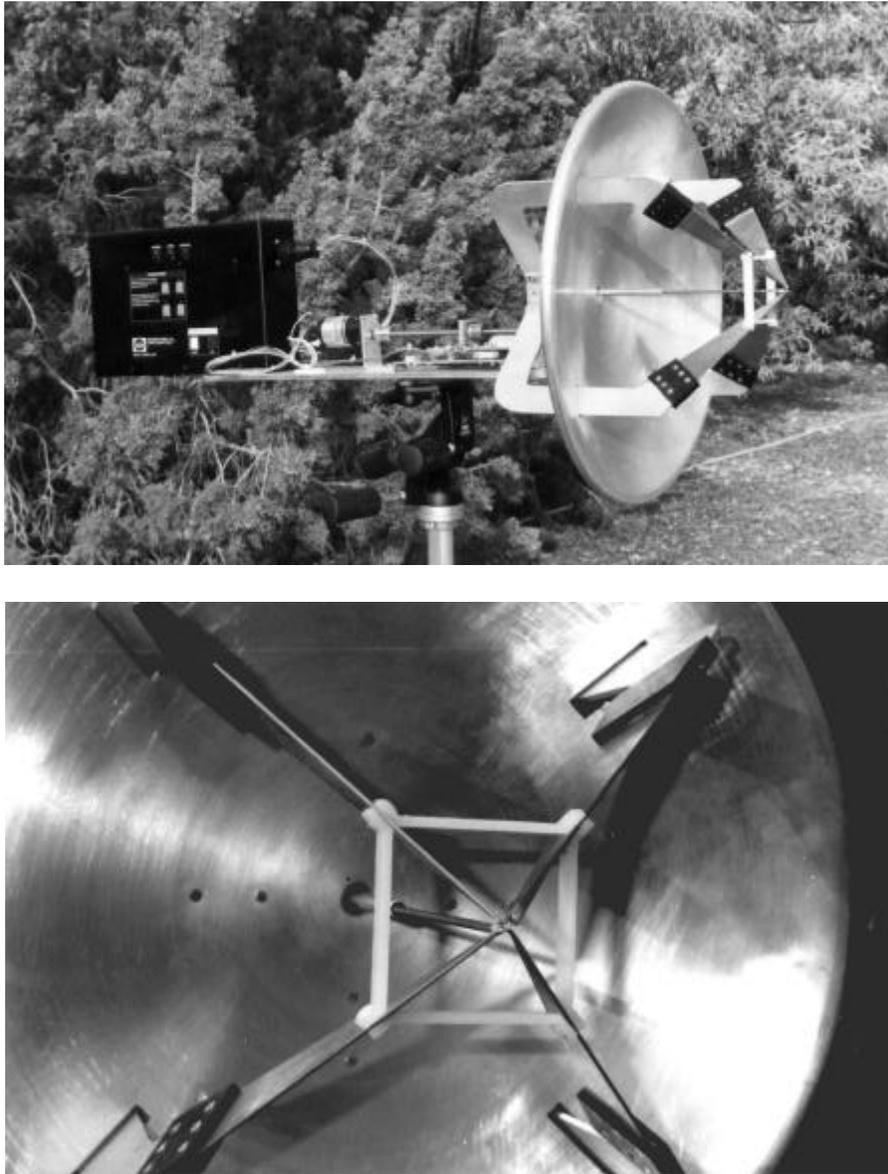
Figure 3.1. The Multifunction IRA, showing the recent modifications.

Raw Voltage, MIRA, Focused

Raw Voltage, MIRA, Focused
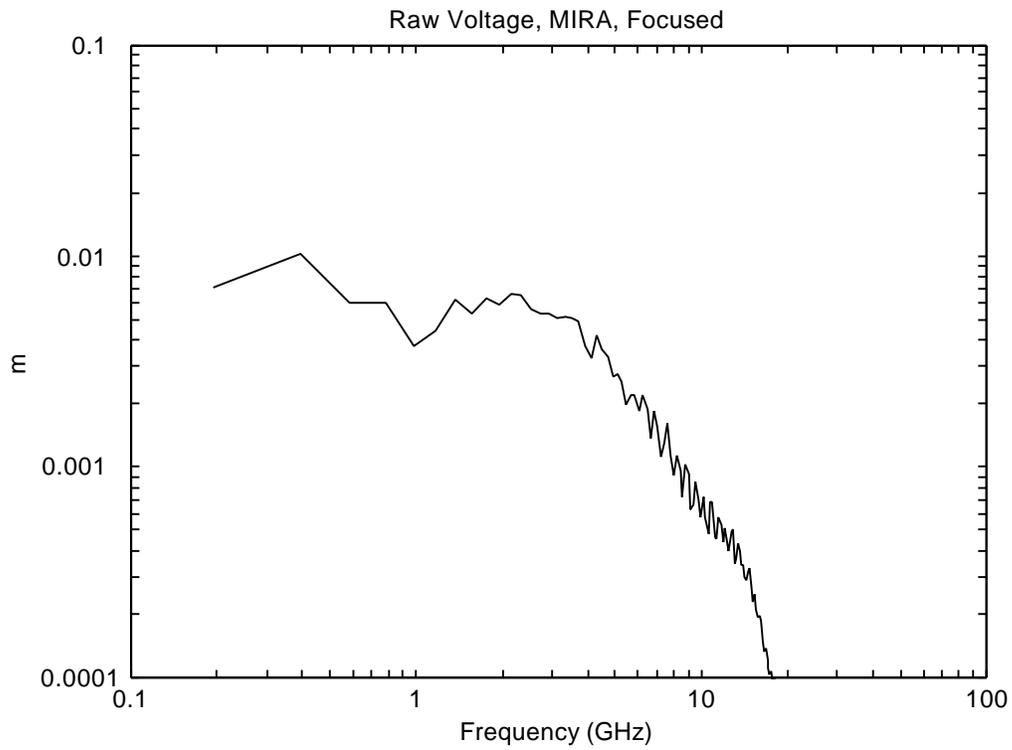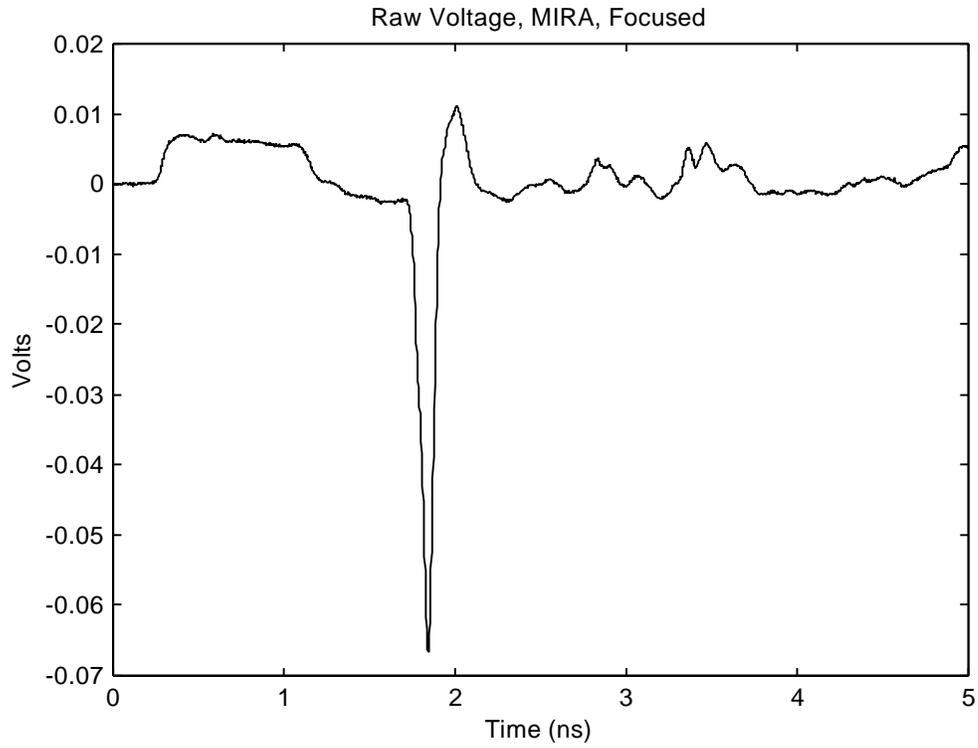
Figure 3.2. Raw voltage response of the MIRA on boresight in the time domain (top) and in the frequency domain (bottom).
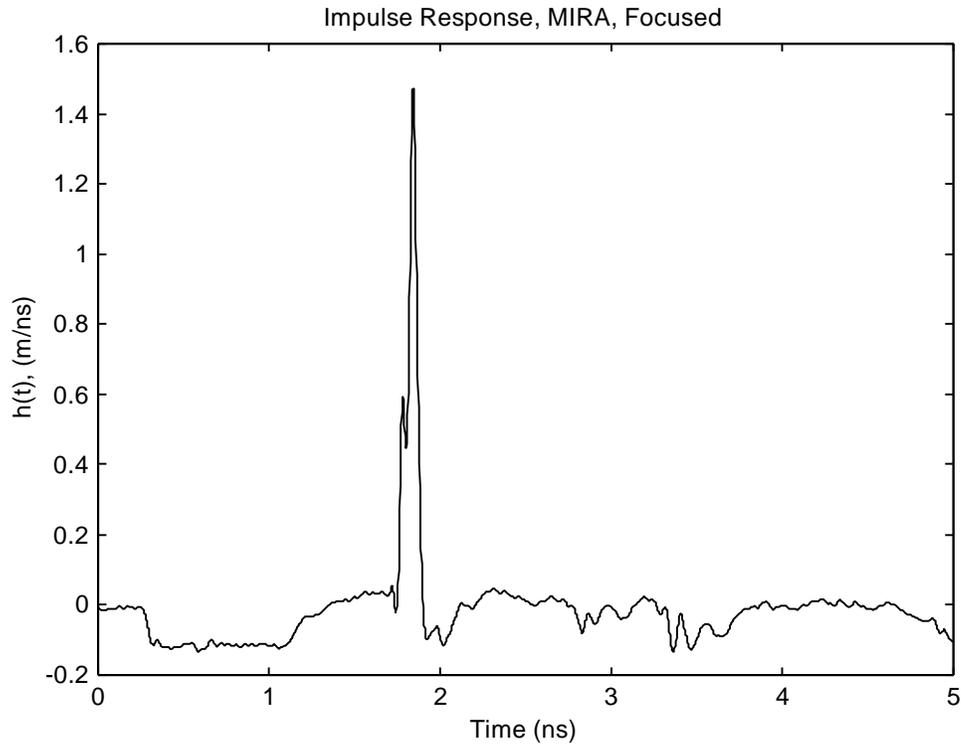
Figure 3.3. MIRA impulse response, $h(t)$, in the time domain (FWHM = 51.6ps).
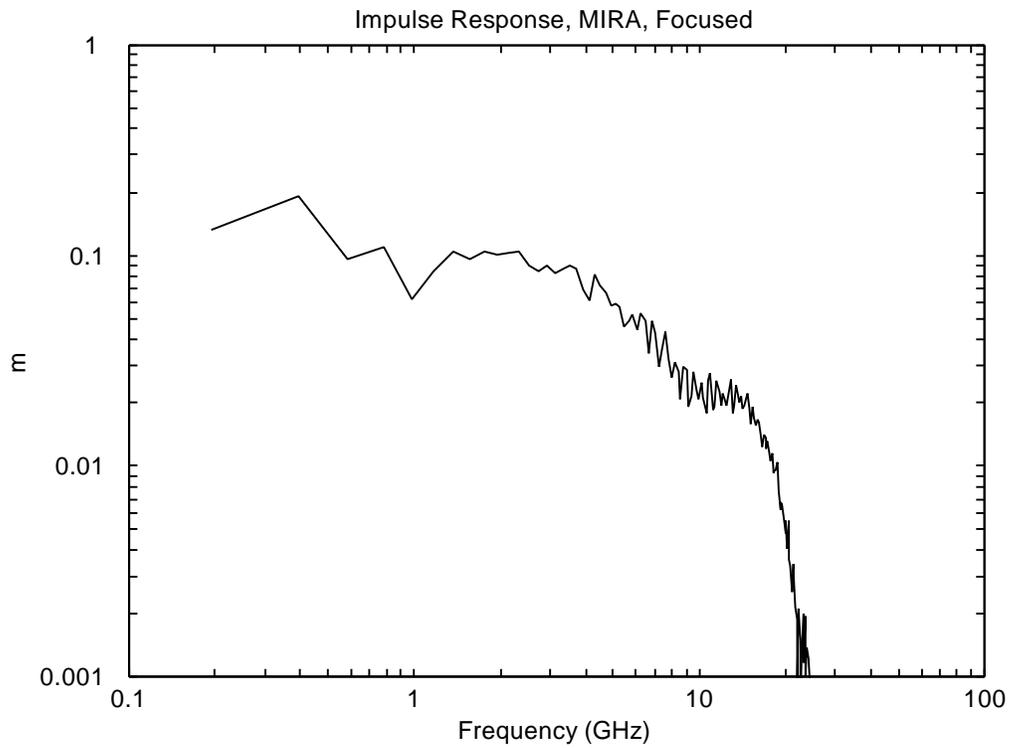
Figure 3.4. MIRA impulse response, $h(w)$, in the frequency domain.
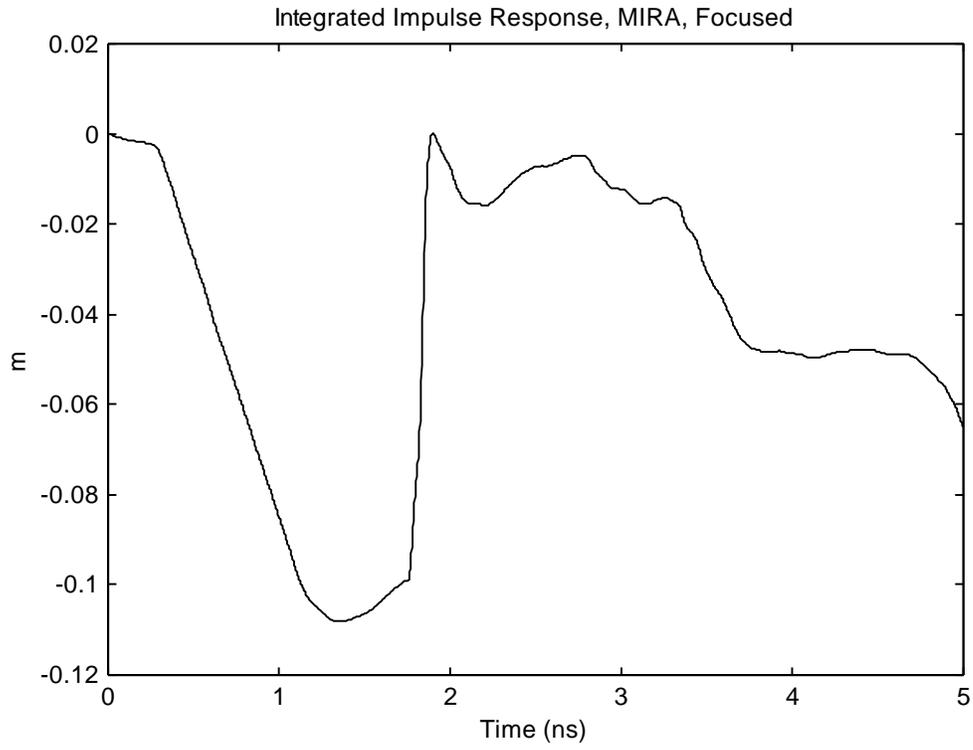
Figure 3.5. Integral of the MIRA impulse response.

H-Plane Scan, Focused
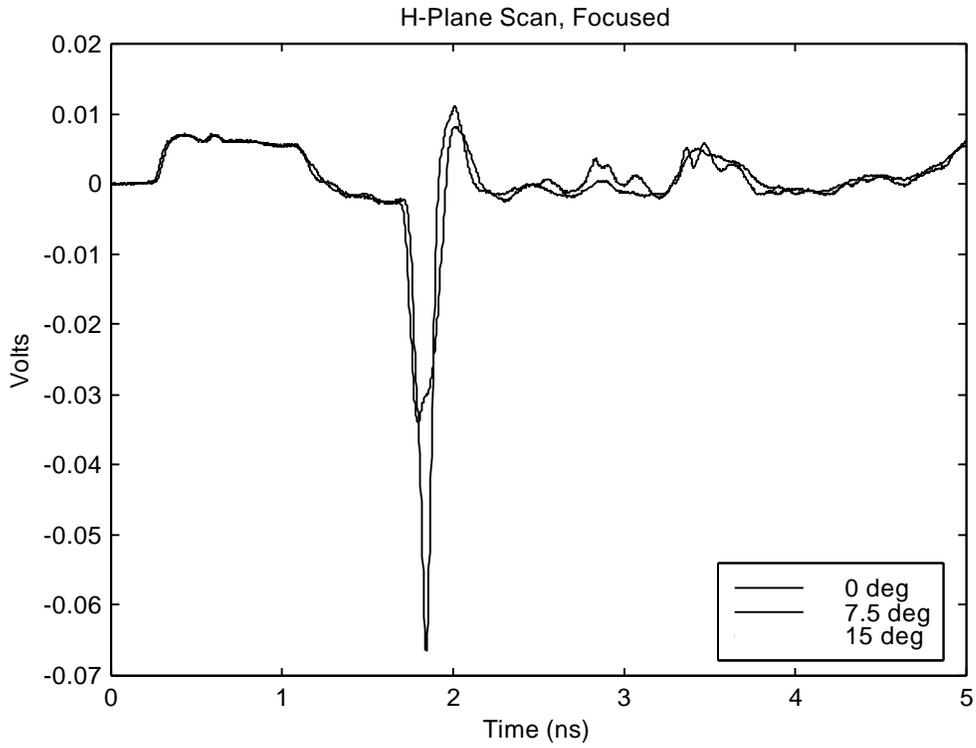
Figure 3.6. H-plane scan of the MIRA antenna response, with $f_f = 1.0$.

H-Plane Scan, Defocused 0.85 F
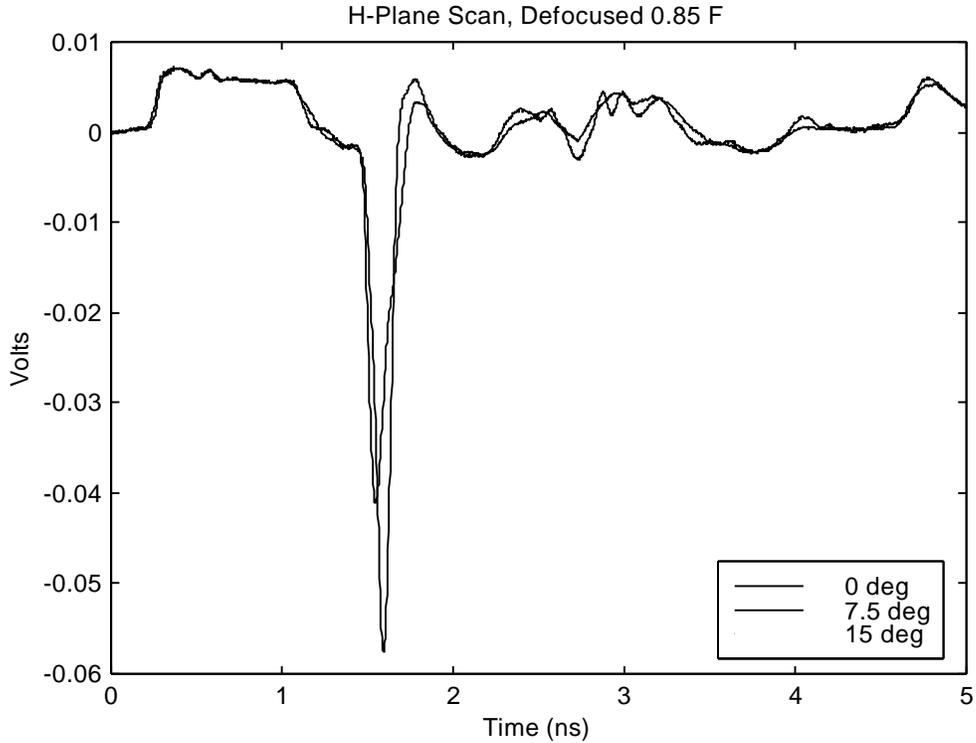
Figure 3.7. H-plane scan of the MIRA antenna response, with $f_f = 0.85$.
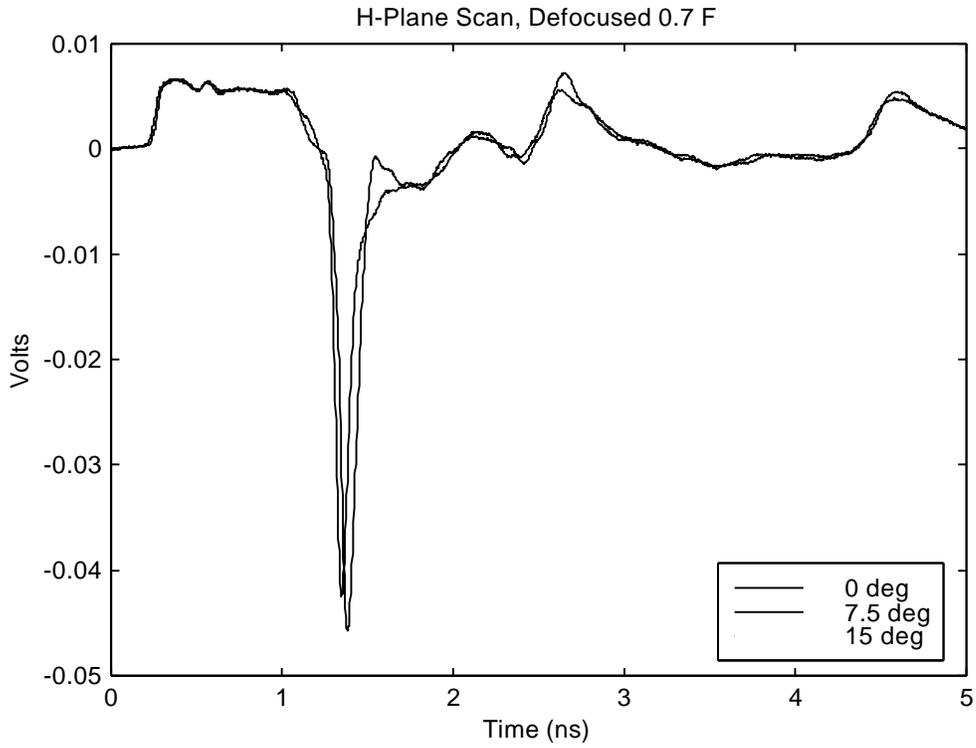
Figure 3.8. H-plane scan of the MIRA antenna response, with $f_f = 0.70$.
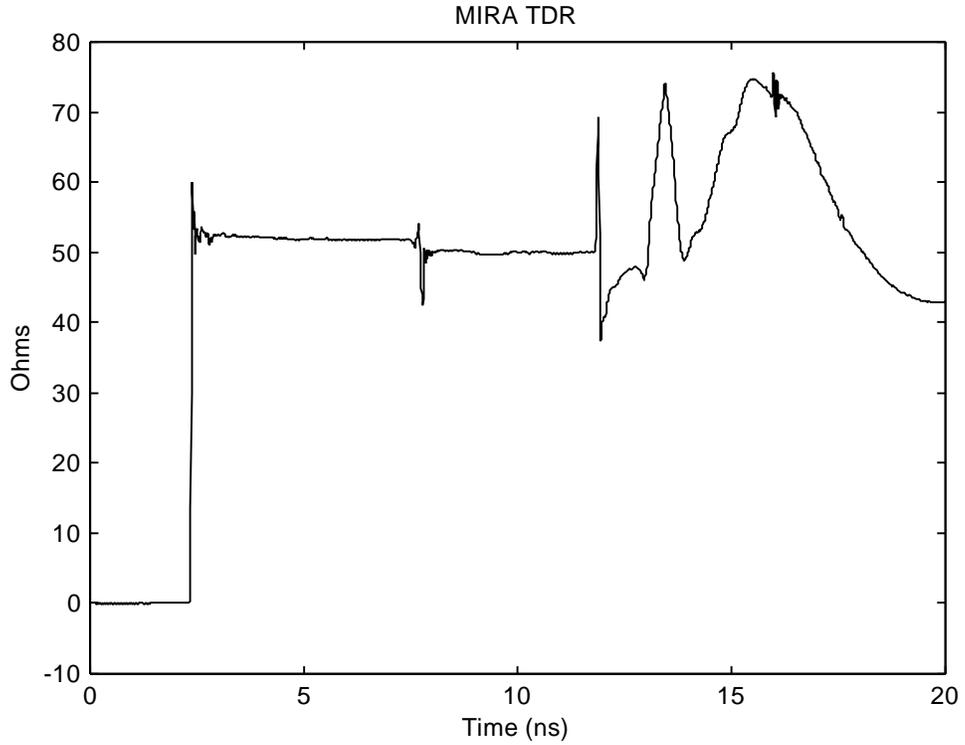
Figure 3.9. TDR of MIRA.

14

IV. Conclusions

Recent modifications of the TEM sensor and MIRA have greatly improved their performance. Additional improvements may be possible, however, several important design considerations can be stated.

Attention to detail at the feed point can greatly improve the performance of both the TEM sensor and MIRA. Extra material (both conductive and dielectric) near the feed point can seriously degrade the performance of the antenna, by producing an impedance mismatch. Other items to be considered are feed element shape and position, and aperture blockage. TDR measurements are quite useful in adjusting the antenna design for optimum performance. Considerable skill is required to provide the required mechanical strength without degrading the electrical response of the antenna.

Four TEM sensors are now available, in two impedances and two sizes. Impulse responses with FWHM as low as 31 ps are available. More complete data on this family of sensors is provided in Table 2.1. These TEM sensors are now commercial products.

Acknowledgements

References

1. E. G. Farr, C. E. Baum, and W. D. Prather, Multifunction Impulse Radiating Antennas: Theory and Experiment, Sensor and Simulation Note 413, November 1997.

2. E. G. Farr and C. E. Baum, Time Domain Characterization of Antennas with TEM Feeds, Sensor and Simulation Note 426, October 1998.

3. E. G. Farr, Optimizing the Feed Impedance of Impulse Radiating Antennas, Part I, Reflector IRAs, Sensor and Simulation Note 354, January 1993.